THE JOURNAL OF PHYSICAL CHEMISTRY C
A JOURNAL OF THE AMERICAN CHEMICAL SOCIETY

pubs.acs.org/JPCC

Article

Enhanced Multiexciton Emission Property in Gradient Alloy Core/Shell CdZnSeS/ZnS Quantum Dots: Balance between Surface Passivation and Strain-Induced Lattice Defect

Hongyu Yang, Lei Zhang, Ying Tang, Wenbin Xiang, Xiaoyong Wang,* Min Xiao, Yiping Cui, and Jiayu Zhang*

Cite This: *J. Phys. Chem. C* 2021, 125, 10759−10767

Read Online

ACCESS | Metrics & More | Article Recommendations | Supporting Information

ABSTRACT: The effect of surface/interface defects on multiexciton recombination is studied with CdZnSeS/ZnS alloy core/shell quantum dots (QDs) with different shell thicknesses. Through pump-power-related time-resolved photoluminescence/amplified-spontaneous-emission (ASE) spectra and statistical analysis of single-dot fluorescence, it is indicated that with the epitaxial growth of the ZnS shell, the multiexciton property of the QDs can be improved due to surface passivation, but with further shell growth, interface defects caused by stress accumulation will result in deterioration. The QDs with three monolayers ZnS shell show the best performance with a biexciton quantum yield of 11.6%, biexciton lifetime of ∼360 ps, and ASE threshold of only 118 μJ cm^{-2}, with which a vertical cavity surface-emitting laser is fabricated. Our experimental results highlight the importance of surface/interfacial defects to the application of QDs on laser devices.

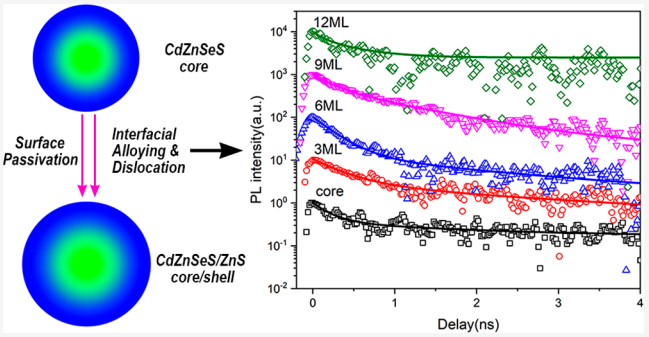

INTRODUCTION

Semiconductor core/shell quantum dots (QDs) exhibit excellent optical performance and stability, which lead to application potential in light-emitting diodes, bioimaging, photovoltaic devices, and low-threshold lasers.[1−4] QDs are important optical gain mediums due to their easily tuned emission spectra, and it is possible to realize full-color lasers with potentially high gain property.[5] However, high densities of excitons for generating optical gain in QDs are easily consumed by the rapid nonradiative Auger recombination (AR) process,[6−8] which leads to low quantum yield (QY) of charged-exciton and multiexciton, thus severely restricting the QD's optical gain performance. The suppression of AR while maintaining high oscillator strength is a long-term goal in the QD's applications, especially for lasers.[4,9] Several researchers have found that the AR process is related to the strength of the Coulomb interaction between carriers and the overlap of the wave functions of the initial and final states involved in the Auger process.[10−12] For single-component QDs, the AR rate, which usually follows the "volume law",[13] is affected by the size and linearly related to the dimension.

Surface defect states will increase the probability of charging of QDs, which will participate in the multiexciton recombination and lead to fast AR and fluorescent blinking, thus possibly inhibiting multiexciton states emission and decreasing the optical gain lifetime.[14−16] Some researches have revealed that the suppression of AR by the growing high-quality CdS shell on the CdSe core results from the effective passivation of the charged state and the surface state. Furthermore, a thick CdS shell can completely suppress the fluorescence blinking due to effective isolation of the surface states. As a consequence, the "giant" CdSe/CdS QDs (up to 20 MLs) have excellent fluoresce properties.[22] However, the CdS shell has finite confinement on the electron, and there is nearly no conduction band offset between CdSe and CdS at room temperature, which makes the delocalization of the electron and captivity by surface defect possible.[17,18] On the other hand, although ZnS material has a wide band gap, growing ZnS shell on CdSe QDs has nearly no improvement on QY and fluorescence blinking,[19,20] which is due to much interfacial defect derived from large lattice mismatch. Thus, it is suggested that a gradient alloy shell with a wide-band gap ZnS material as the final shell could reduce surface/interfacial defects. Currently, core/shell QDs synthesized by increasing the Zn^{2+} density at the interface, such as CdSe/$Cd_{1-x}Zn_xS$,[21,22] CdSe/Cd_xZnSe_{1-x}/$ZnSe_{0.5}S_{0.5}$,[23,24] and CdZnSe/ZnSe/ZnS,[25,26] can

Received: March 7, 2021
Revised: May 1, 2021
Published: May 10, 2021

https://doi.org/10.1021/acs.jpcc.1c02029
J. Phys. Chem. C 2021, 125, 10759−10767

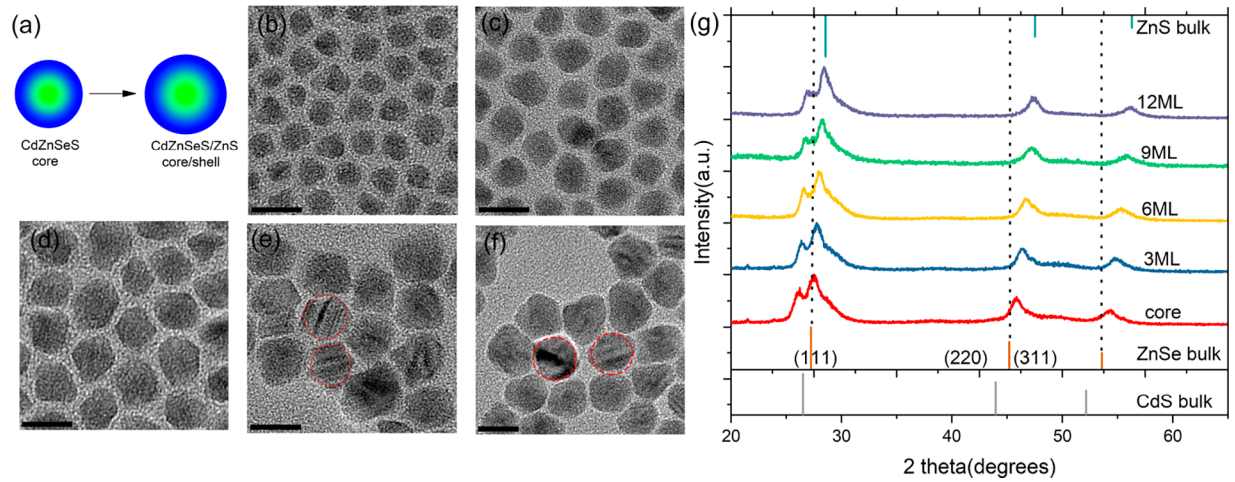

Figure 1. (a) Schematic description of the CdZnSeS/ZnS gradient alloy QDs. (b)−(f) The corresponding TEM of #core, #3 ML, #6 ML, #9 ML, and #12 ML. The red circles depict the obvious lattice-stacking faults. (g) Their X-ray diffraction patterns. The standard diffraction patterns of bulk CdS, ZnSe, and ZnS with zinc-blended structure are given as references.

effectively eliminate the defect state caused by the lattice mismatch during the growth process, so the AR process involving traps can be significantly suppressed.[27−29]

Although utilizing a thick ZnS shell as a final passivation layer is a target, the strain accumulation during the growing process is still large, increasing the possibility of forming interfacial defects. Thus, the AR rate may be increased, and the blinking events become more often. The recombination of the multiexciton in QDs includes the following: (a) radiative combination of band-edge electron−hole pairs, (b) trapping process where interfacial defects or surface defects serve as nonradiative centers, and (c) nonradiative AR.[27] The process in which interfacial traps are involved in AR by coupling with other band-edge carriers is very fast (∼20 ps) due to the high spatial confinement, which leads to high momentum components so that momentum conservation constraints need to be relaxed.[30] Previous studies have shown that the density and location of interfacial defects can also affect the charging probability of QDs.[27,31,32]

In this paper, the gradient alloy CdZnSeS QDs were prepared by a "one-pot" method, and then their surface was gradually epitaxially grown with ZnS shell to further passivate the surface. Our experimental results show that the ZnS shell with 3 monolayers (MLs) thickness could prolong the biexciton lifetime and reduce the ASE threshold, but further coating will introduce more interface defects, resulting in a decline in their optical properties. The analysis of the single-dot fluorescence trace and biexciton decay curve indicates the importance of reducing interfacial defects on the optical gain. The high-performance gain medium is further proved by fabricating a VCSEL with a threshold of ∼100 μJ cm^{-2}.

EXPERIMENTAL SECTION

Chemical. Cadmium oxide (CdO, 99.998%), oleic acid (OA, technical grade, 90%), zinc oxide (ZnO, 99%), tri-n-octylphosphine (TOP, 98%), and sulfur (S, 99.98%) were purchased from Aldrich. 1-Octadecene (1-ODE,90%) and Se (200 mesh, 99.999%) were purchased from Alfa-Aesar. All the chemicals were used without further purification.

Synthesis Method. The gradient alloy CdZnSeS QDs were prepared according to a previously published method with slight modification.[33,34] Briefly, 6.82 mmol of ZnO, 0.28 mmol of CdO, 14 mL of OA, and 30 mL of ODE were added in a three-necked bottle. It was degassed under 130 °C using a Schlenk-line for 1 h, and then the temperature was raised to 310 °C until the solution became transparent to produce the cation precursors of $Cd(OA)_2$ and $Zn(OA)_2$. Transparent anion precursors prepared by dissolving 4.4 mmol of Se and 4.4 mmol of S with 4 mL of TOP were injected quickly, and the core growth lasted 10 min. To grow the ZnS shell, a solution prepared by dissolving 3.2 mmol of S in 4.8 mL of ODE was injected and reacted for 12 min. The shelling anion precursors were prepared by dissolving S in TOP (1.93M), and cation precursors were prepared by dissolving 11.44 mmol of $Zn(Ac)_2$ in 8 mL of OA and 16 mL of ODE. Further, the different thick ZnS shells were prepared by injecting different amounts of Zn and S precursor, and then the reaction was annealed for 20 min at 270 °C. The synthesized QDs were purified repeatedly by a precipitation/dispersion method and dispersed in nonpolar organic solvents for further characterization.

Material Characterization. The absorption spectra were recorded using a Shimadzu UV-3600 spectrometer; PL spectra were measured using a Shimadzu RF-5301PC spectrometer. The PL quantum yield was compared with standard Rhodamine B dye with the same optical density. TEM images were acquired using a JEOL company JEM-2100 electron microscope, with an acceleration voltage of 20 kV. X-ray diffraction patterns were measured using a Rigaku D/max 2500/PC X-ray diffractometer operating at theta/2theta mode using the Cu−Kα line (λ = 1.5418 Å).

Transient time-resolved measurement of QD solution was performed with a Hamamatsu C5680 streak camera working in slow single-sweep mode, excited by frequency-doubled femtosecond laser using β-BBO of a Ti:sapphire laser system (800 nm, 150 fs,1 kHz, Coherent Legend F-1k). Single-dot fluorescence was measured by a confocal microscopy system. The diluted QD solution was mixed with the toluene solution of polylactic acid and then spin-coated on the quartz substrate. The picosecond supercontinuum fiber laser (405 nm, 4.9 MHz, NKT Photonics EXR-15) was used as the excitation source, and the excitation density was 1 W cm^{-2}. The fluorescence was collected through the excited objective lens. ASE spectra were collected at the edge of the film with fiber

https://doi.org/10.1021/acs.jpcc.1c02029
J. Phys. Chem. C 2021, 125, 10759−10767

and analyzed using an optical multichannel analysis instrument (OMA, Spectrapro-300i, Acton research corporation) with a grating period of 300 g/mm. The transient decay processes were measured using the streak camera mentioned above working in the synchroscan mode. VCSEL was pumped using the aforementioned laser with a lens of 10 cm focus length. Laser spectra were collected with the OMA with a grating period of 1200 g/mm.

RESULT AND DISCUSSION

Gradient alloy CdZnSeS QDs were synthesized by the "one-pot" method[33] with some modifications (see the Experimental Section). Briefly, four different precursors ($Cd(OA)_2$, $Zn(OA)_2$, TOP-Se, and TOP-S) dissociated at 310 °C, forming a CdSe-rich core and ZnS-rich shell with gradient alloy interface according to the reactivity and concentration of the precursors as the reaction proceeded. The Cd/Zn and S/Zn molar ratios were 4.1% and 64.5%, respectively, to participate in the reaction. To cap the surface further, $Zn(OA)_2$ and TOP-S were utilized as precursors to epitaxially grow a wide-band ZnS shell. The transmission electron microscopy images of the as-prepared QDs are shown in Figure 1a. The shapes of the QDs were relatively regular due to the high growing temperature.[35] The average size of the CdZnSeS core was ~10.2 nm, and the size of the core/shell QDs increased to 12.8, 14.7, 16.5, and 18.1 nm as the shell grew , which corresponded to about 3, 6, 9, and 12 MLs. Moreover, obvious stacking faults can be observed in the TEM image shown in Figure 1e and f, which are the signs of strain release at the interface. Hereafter, these samples are labeled as #core, #3 ML, #6 ML, #9 ML, and #12 ML. The X-ray diffraction (XRD) patterns, as shown in Figure 1b, indicate a zinc-blend crystal structure and well crystalline quality with sharp peaks. Calculated according to position of the (220) diffraction peak, the lattice constants of these QDs are 1.9734, 1.9519, 1.9372, 1.9235, and 1.9155 Å, respectively. The lattice constant of the core is closer to ZnSe (2.0046 Å) because the Zn/Cd molar ratio is very high. Cd precursor was consumed mainly forming CdSe, and the reactivity of TOP-S was far lower than that of TOP-Se, so Zn precursor reacted with a large amount of TOP-Se and a gradient ZnSe-rich alloy interface was formed. Because the lattice mismatch of ZnSe and the subsequently growing ZnS (1.9120 Å) shell is small, the formed strain can be small as well.[36,37] Upon the growth of the ZnS shell, the diffraction peaks of nanocrystals gradually narrow and shift from the ZnSe pattern to that of ZnS, which proves successful ZnS shell growth and the compressive stress on the core.

Figure 2a presents the evolution of the UV−vis absorption and photoluminance (PL) spectra of these QDs measured at room temperature. With the growth of the ZnS shell, the PL full width at half-maximum (fwhm) remains as narrow as ~23 nm due to the effective quantum confinement effect of ZnS and QD's narrow size distribution. Both PL and first exciton absorption (1S) peaks are blue-shifted, while the absorption between 300 and 350 nm is increased obviously due to the epitaxial growth of the ZnS shell. The PL/absorption blue-shift may be caused by increasing quantum confinement as the shell grows and in situ alloying of the core with ZnS.[38,39] The QY value is increased from 40% of #core to 85% of #3 ML because the high synthesis reaction temperature causes Zn ions to diffuse into the surface of the CdZnSeS core. As a consequence, the growth of the shell forms a continuous lattice parameter change from the core to the shell without the formation of structural defects. Upon further shelling with 6, 9, and 12 ML, the QY values are decreased toward 75%, 63%, and 35%. This can probably be attributed to the interfacial dislocations resulting from the release of the accumulated lattice strain, which will serve as nonradiative centers.

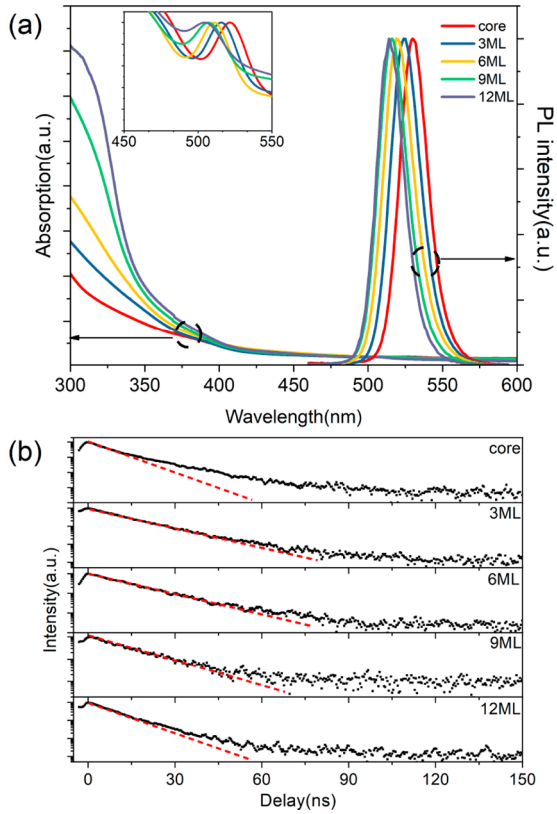

Figure 2. (a) UV−vis absorption and PL spectra of all samples; the inset shows the variance of the 1S absorption. (b) The corresponding PL decay traces (dots) and the single-exponential fitting curves for the initial stage (red dashed line).

Figure 2b shows the PL decay trace under weak excitation ($\langle N \rangle$ = ~0.01), where the red dashed lines show the band-edge exciton combination process and the fluorescence decay trends are consistent with that of QY. The decay trace of #core deviates far from single-exponential decay with a long tail, which is related to the interaction of the exciton and surface defect states.[22,31] This indicates that the surface of #core is not perfectly passivated.[34] The decay curves of #3 and #6 could be well fitted with a single-exponential because of the ZnS shell growth with almost no interfacial defect. However, with further shell growth, the decay traces deviate again from the single-exponential decay. This is due to the appearance of the interfacial dislocation, which could be obviously seen in the red dashed circles in Figure 1e and f. Figure 2 indicates that the QD's surface could be well passivated by the epitaxial of the ZnS shell, but a shell thicker than 6 ML ZnS will introduce nonradiative interfacial traps.

PL intensity trajectories of single QDs were measured at room temperature for these samples, depicted in Figure 3a and Figure S1. The threshold line is positioned at ~15% lower in intensity relative to that of the "on"-level central peak to minimize the overlap between the two events and collect enough data for further analysis. As is shown in the corresponding histogram, the #core has clear two-step binary blinking with well-defined "on" and "off" states. In comparison,

https://doi.org/10.1021/acs.jpcc.1c02029
J. Phys. Chem. C 2021, 125, 10759−10767

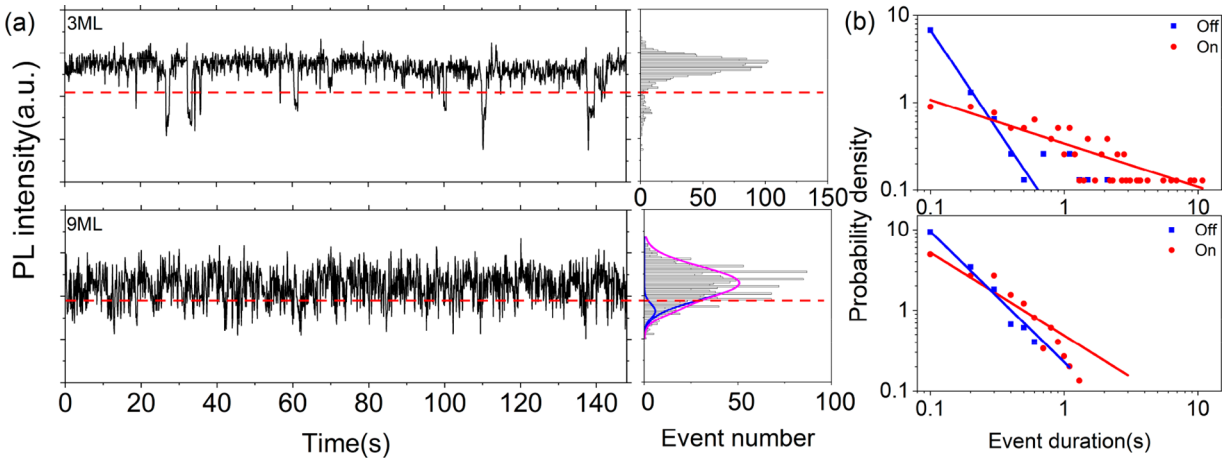

Figure 3. (a) Typical single-dot fluorescence traces of #3 ML and #9 ML samples under 405 nm picosecond pulse excitation; the right shows intensity distribution histograms. Binning time: 100 ms. The threshold set 15% lower than the peak of on states is depicted using the red dashed line. (b) Corresponding log–log plot of probability density distributions of on and off events.

#3 ML, #6 ML, and #9 ML samples have obvious effects on surpressing the off event, and #12 ML sample has a long period off event. The probability statistics for the duration of on and off events were caculated according to the blinking traces, which satisfy a power-law distribution[40] ($P \propto t^{-\mu}$ with t as the duration of a period and μ as the power-law coefficients), as depicted at the right of corresponding intensity traces in Figure 3b and Figure S1b. The fitted results are shown in Figure S2, where the smaller coefficient proves the slower decrease trend of probability and longer event probable.[31,41] For #core sample, $\mu_{on/off}$ = 1.1/1.29, and long duration periods of both on and off events are due to surface defects. Upon shelling to 3 ML, the coefficients $\mu_{on/off}$ = 0.5/2.27 prove that the longer on event duration is more favorable and the off duration decays very fast. Subsequent shell coating makes the μ_{on} value increase and that of μ_{off} decrease. Fluorescence blinking behavior generally comes from efficient nonradiative AR and defect state trapping.[14,19] A thin shell with only 3 ML has a greater probability of being in the on state for a long period than the core itself and with a thicker shell, which proves efficient suppressed nonradiative AR and perfect surface passivation without interfacial defects. On the contrary, the subsequent shelling introduces more lattice strain and increases the interface defect density.

To study the recombination dynamics of multiexcitons within QDs, the time-resolved PL was measured as a function of excitation intensity, as shown in Figure 4 and Figure S3. Under high-power pump intensity, a fast-decay component (in subnanosecond scale) emerges for all the QDs, which is a typical signature of multiexciton recombination.[12,15] The PL decay traces of 3 ML with increasing pump fluence exhibit the following characteristics: (1) The fluorescence intensity in the initial fast stage is increased approximately linearly with the increase of the pump power. When the surface of the QDs is not passivated (#core) or coated with a thick shell with introduced defects (#9 and #12), the fluorescence increase with the pump power will deviate from linearity. This is due to the surface/interface defects serving as a nonradiative center. (2) The intensity of the decay curve tail component will tend to saturate under a high-power pump. It is suggested that the multiexcitons in II–VI semiconductor QDs could completely decay within 0–5 ns, leaving only single-exciton fluorescence.[12,42] The inset in Figure 4a shows the dependence of the

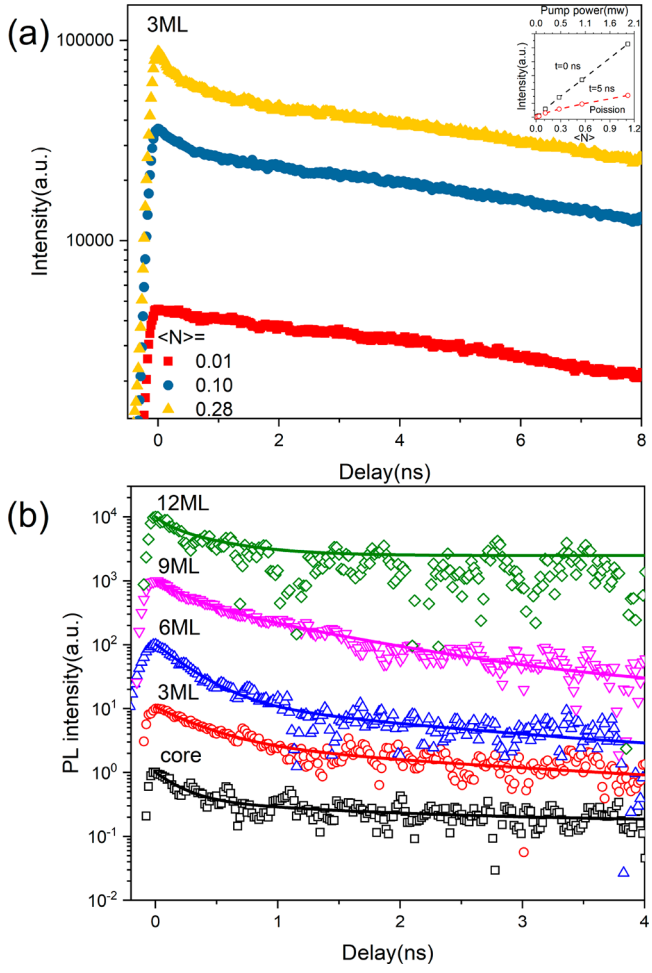

Figure 4. (a) Pump-power-dependent PL decay dynamics of #3 ML; the inset shows the dependence of PL intensity at time delays of 0 and 5 ns on ⟨N⟩ and pump power. (b) The initial fast-decay dynamics extracted from the "tailor-normalized" at t = 5 ns with ⟨N⟩ = 0.1 and 0.01 of all samples.

fluorescence intensity at t = 5 ns on the pump power, which could be fitted using the following equation:[43] $I_{long} \propto e^{-j\delta_{abs}}$, where j is the pump intensity and δ_{abs} denotes the absorption cross section at 400 nm. The δ_{abs} value, obtained by fitting the

https://doi.org/10.1021/acs.jpcc.1c02029
J. Phys. Chem. C 2021, 125, 10759–10767

Table 1. Photophysical Properties of All QD Samples

sample	τ_x (ns)	τ_{xx} (ps)	τ_{x^*} (ns)	QY_{xx} [a](%)	$\tau_{xx,Auger}$ [b](ps)	$\tau_{x-,Auger}$ [c] (ns)	$\tau_{x+,Auger}$ [c] (ns)
#core	9.43	195.7	1.41	8.30	202.42	1.61	0.54
#3 ML	12.41	359.6	2.78	11.59	398.9	4.49	0.97
#6 ML	13.96	263.6	2.00	7.55	279.43	2.55	0.72
#9 ML	12.38	231.9	1.08	7.49	243.39	1.22	0.81
#12 ML	9.48	–	0.46	–	–	–	–

[a]Biexciton QY was calculated according to $QY_{xx} = 4\tau_{xx}/\tau_x$ based on the assumption that the radiative biexciton lifetime is 4 times shorter than the single-exciton lifetime.[9] [b]Biexciton Auger lifetime was obtained according to $\tau_{xx,A}^{-1} = \tau_{xx}^{-1} - \tau_{xx,r}^{-1}$, where $\tau_{xx,r} = \frac{\tau_{x,r}}{4}$ and $\tau_{x,r} = \frac{\tau_x}{QY_x}$;[48] [c]The biexciton Auger process can be treated as resulting from superposition of two independent channels associated with positive and negative trion pathways,[42] and the biexciton lifetime satisfies the following relationship: $\frac{1}{\tau_{xx,A}} = 2\left(\frac{1}{\tau_{x+,A}} + \frac{1}{\tau_{x-,A}}\right)$. The trion Auger lifetime can be calculated according to $\frac{1}{\tau_{x-/+}} = \frac{1}{\tau_{x-/+,A}} + \frac{1}{\tau_{x-/+,r}}$ and $\tau_{x-,r} = \tau_{x,r}/2$.[46,48]

curves in Figure 4 and Figure S3, is on the order of $\sim 6 \times 10^{-15}$ cm^{-2} for all samples. It is generously suggested that when the average number of excitons ($\langle N \rangle = j\delta_{abs}$) in QDs is not greater than 0.1 (corresponding to the pump power ~8 μJ cm^{-2}), there are only single-excitons and biexcitons in the QDs during the initial decay stage, and there are no other multiexciton states such as triple-exciton.[28] The biexciton or trion radiative decay curve could be acquired by extracting the fast-decay component with $\langle N \rangle$ = 0.1 from $\langle N \rangle$= 0.01, because it is supposed that in the case of $\langle N \rangle$ = 0.01 there are only single-excitons in QDs, as shown in Figure 4b and Figure S4b. These curves could be well fitted with a biexponent function, corresponding to the recombination process of biexciton and negatively charged trion,[44] respectively. In asymmetric confinement of electrons and holes for QDs, ARs are dominated by the fast positive-trion pathway,[45] such that the recombination energy of the biexciton is transferred to a highly localized hole. This specific AR channel also lead to the Auger ionization process dominated by hole ejection of QDs and leave behind an uncompensated electron forming a negative trion.[27,46] In conclusion, the negative trions are formed after the initial photon excitation. (3) The measurement data about the fluorescence features are summarized in Table 1 for all five samples. Biexciton emission is negligible in #12 sample even at $\langle n \rangle$ = 0.4. The trion lifetime of 3 ML is almost twice that of the core, indicating the successful surface passivation and the suppresion of trion recombination through the AR process. For thick-shell QDs, the trion recombination rate through AR is accelerated. The fitted results are summarized in Table 1.The biexciton Auger lifetime (τ_{2A}) of 3 ML is almost twice of that of #core, whereas it does not follow the universally accepted statistical scaling observed in monocomponent and thin-shell QDs[6] when the shell thickness is further increased, proving the multiple nonradiative AR pathway in thick-shell QDs.

It is supposed that the AR process often takes place at the interface between the core and shell and is sensitive to the sharpness of the interface potential.[47] Alloying at the interface could reduce the AR rate by about 3 orders of magnitude, as a result of potential softness and reducing the chance of localization of the electron−hole wave function at the alloy interface, thus reducing its contribution to higher-order momentum and the probability of AR. Moreover, it is also suggested that surface/interfacial traps could affect the AR process. The carriers captured by these defects are highly localized and basically eliminate the momentum prohibition condition of AR,[27,48] so they are easily coupled with band-edge excitons and involved in the AR process. A previously published result by our group[49] has shown that different from CdSe/CdS QDs, the main defects in CdZnSeS/ZnS QDs are electron traps, with thicker shells and more trap densities. Considering this, we think that the electron trap may also involve the AR and influence the trion AR lifetime.[42,46] It is worth noting that $\tau_{x+,A}$ and $\tau_{x-,A}$ of 3 ML are about 2 and 2.8 times that of the core, indicating that the Auger process is effectively suppressed. Further shelling decreases the Auger lifetime of the trion, especially for the negative trion. The value of $\tau_{x+,A}$ decreases but still is larger than the core, proving that the increase of the electron trap density is the main reason for the shorter biexciton lifetime and decrease of QY_{xx}.

To further study the multiexciton emission of QDs, we measured the amplified spontaneous emission (ASE) under stripe excitation. Uniform QD film with ~260 nm thickness was prepared by spin-coating on a glass substrate to form a planar waveguide structure, whose atomic force microscope (AFM) image is shown in the inset of Figure 5a. Its root-mean-square (~3 nm) and peak-to-peak surface roughness (~28 nm) are much smaller than the excitation and emission wavelengths, so there are no randomly formed cavities, which could confuse QD's intrinsic optical gain characteristics. The pump beam (400 nm, 150 fs, 1 kHz) was focused through a cyclical lens into 50 μm*4 mm strips on the film. For #core sample, it can be seen that a clear threshold (~184.4 μJ cm^{-2}) distinguishes linear spontaneous emission from superlinear ASE and spectra narrowing (fwhm = ~5 nm), which are the features of ASE. The ASE position of the QDs has a red shift (~7.5 nm) relative to the spontaneous emission peak, resulting from the attraction between excitons of type-I QDs and the thickness-related mode selection effect.[50,51] For #3 ML sample, the threshold is decreased to 118.2 μJ cm^{-2}. Upon further shelling to 6 and 9 ML, the ASE threshold increased to 164.8 and 213.3 μJ cm^{-2}. Moreover, the relative decrease of overlap between the electron and hole wave function is proved by the smaller red shift (~5 nm) due to the further alloy in the interface and the change of biexciton combination energy. By the way, for #12 ML sample, no ASE behavior could be observed even if the pump intensity was increased toward 900 μJ cm^{-2}, and the emission peak did not shift, mainly due to the large defect density serving as a nonradiative center, which accelerates the AR process.

The transient spectra of the #3 ML sample's ASE are shown in Figure 6a. Under low pump intensity (~60 μJ cm^{-2}), we only observe a broad-spectrum spontaneous emission peak with long-lived lifetime (>3 ns). With the increase of the pump intensity toward 120 μJ cm^{-2}, a narrow ASE peak and rapid

https://doi.org/10.1021/acs.jpcc.1c02029
J. Phys. Chem. C 2021, 125, 10759−10767

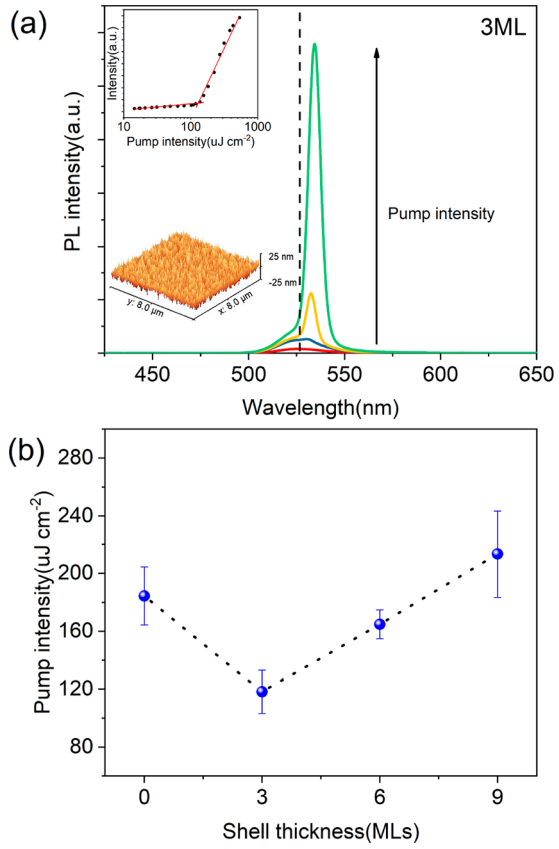

Figure 5. (a) Pump-intensity-dependent ASE spectra of #3 ML QDs film; the inset presents the AFM image of the QD film's surface (below) and the evolution of the integrated emission intensity as a function of the pump intensity, showing superlinear behavior over the threshold. (b) Average threshold of all samples.

decay component (~35 ps) appear. When the excitation intensity is increased over the ASE threshold, the fast-decay lifetime is further shortened to ~13 ps, which is ~30 times shorter than the Auger lifetime. This process is fast enough to compete with the fast AR, indicating that the #3 ML sample is an effective laser material.

A vertical cavity surface emitting laser (VCSEL) containing the #3 ML QDs was fabricated by drop casting high-concentrated (~100 mg/mL) hexane/octane (v/v = 5:1) QD solution to form a thick film (~52um) as the gain material on a distributed Bragg reflector (DBR) with refractivity more than 99% ranging from 465 to 605 nm, as depicted in Figure 7a. Then, ~300 nm SiO_2 and 60 nm silver film were deposited by using thermal evaporation. SiO_2 layer was used to protect the QD's excitons characteristic from absorption of silver. Under low pump intensity, many narrow fluorescence peaks appear in the microcavity spectra (~3 nm), which are obvious Fabry–Perot resonances. The resonance peaks can be assigned according to the following equation:[52] $m\lambda = 2L_{effective}$, where m = 101–106 is the resonance number and λ is the emission wavelength; $L_{effective} = \lambda^2/\Delta\lambda$ is the effective microcavity length.[53] Figure 7b shows the fluorescence intensity spectra of the microcavity under different pump intensities. When the pump intensity is over the threshold (~100 uJ cm^{-2}), the fwhm of mode number 103 and 104 is narrowed to ~1.1 nm with the abrupt increase of the modes' output intensity as shown in the inset of Figure 7b. These two modes are all in the range of the ASE spectrum, which consumes most of the population inversion that these modes can lase. The spatially coherent emission of a laser beam[15] was observed here with a bright spot on the plane 5 cm behind the cavity. The quality factor of the microcavity ($Q = \frac{\lambda_0}{fwhm}$) is ~510.

CONCLUSION

In conclusion, we used a one-pot method to prepare the gradient alloy structure CdZnSeS QDs coated with different thicknesses of ZnS shell and systematically studied the effect of ZnS shell thickness on the QD's multiexciton emission characteristics. Due to the effective passivation and finite lattice strain without forming interfacial defects, blinking and AR process are suppressed in the case of 3 ML ZnS shell, and its ASE threshold is decreased toward ~106.7 μJ cm^{-2}. Taking advantage of the excellent gain characteristics of these QDs, a low-threshold (100 μJ cm^{-2}) spatially coherent multimode laser is obtained. Moreover, a thick shell will lead to stress accumulation that induces more interfacial defects, which increases the probability of trapped multiple excitons and

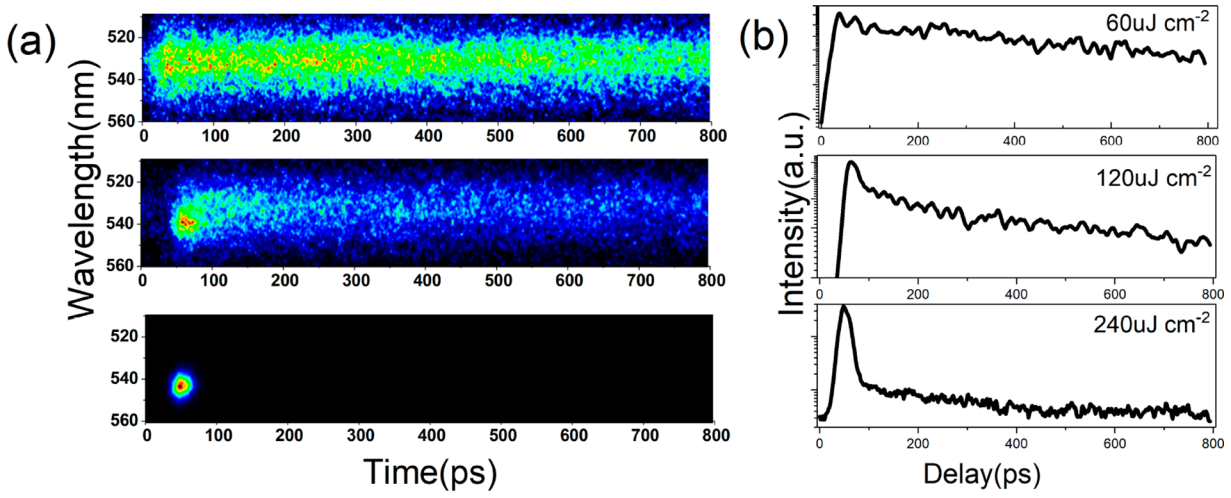

Figure 6. Evolution of transient spectra of #3 ML QD's film with different pump power. The right plot shows the corresponding decay trace at the ASE peak (~540 nm).

https://doi.org/10.1021/acs.jpcc.1c02029
J. Phys. Chem. C 2021, 125, 10759–10767

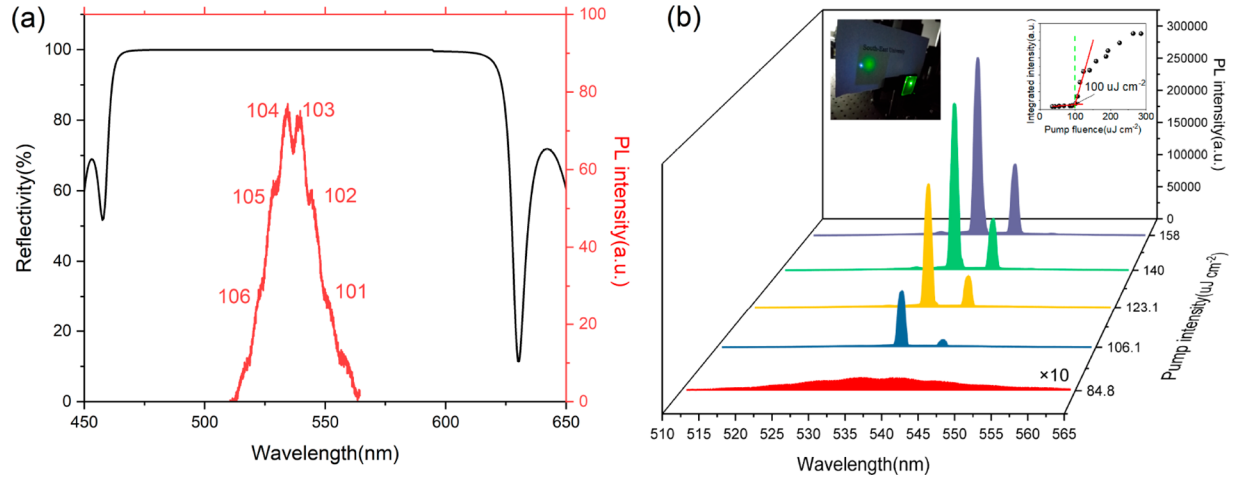

Figure 7. (a) Reflectivity spectrum of the DBR and photoluminance of the microcavity under low pump intensity (~30 μJ cm^{-2}).The numbers indicate the Fabry–Perot microcavity resonance mode. (b) VCSEL emission as a function of pump fluence; the inset shows the photograph of laser emission and pump-fluence-dependent emission intensity.

reduces the gain properties. This work provides an excellent thin-shell CdZnSeS/ZnS as a green color gain material, which can be utilized in realistic laser devices.

■ ASSOCIATED CONTENT

Supporting Information

The Supporting Information is available free of charge at https://pubs.acs.org/doi/10.1021/acs.jpcc.1c02029.

Single-dot fluorescence trace of #core, #6 ML, and #12 ML sample with corresponding intensity distribution histograms and P_{on} and P_{off} distribution; event duration probability fitted results of μ_{on} and μ_{off}; PL decay traces and ASE spectra of #core, #6 ML, #9 ML, and #12 ML with increasing pump fluence (PDF)

■ AUTHOR INFORMATION

Corresponding Authors

Xiaoyong Wang – *National Laboratory of Solid State Microstructures, College of Engineering and Applied Sciences, and School of Physics, Nanjing University, Nanjing 210093, China;* orcid.org/0000-0003-1147-0051; Email: wxiaoyong@nju.edu.cn

Jiayu Zhang – *Advanced Photonics Center, Southeast University, Nanjing 210096, Jiangsu, China;* orcid.org/0000-0001-7868-6346; Email: jyzhang@seu.edu.cn

Authors

Hongyu Yang – *Advanced Photonics Center, Southeast University, Nanjing 210096, Jiangsu, China*

Lei Zhang – *Advanced Photonics Center, Southeast University, Nanjing 210096, Jiangsu, China*

Ying Tang – *National Laboratory of Solid State Microstructures, College of Engineering and Applied Sciences, and School of Physics, Nanjing University, Nanjing 210093, China*

Wenbin Xiang – *Advanced Photonics Center, Southeast University, Nanjing 210096, Jiangsu, China*

Min Xiao – *National Laboratory of Solid State Microstructures, College of Engineering and Applied Sciences, and School of Physics, Nanjing University, Nanjing 210093, China; University of Arkansas, Fayetteville, Arkansas 72701, United States*

Yiping Cui – *Advanced Photonics Center, Southeast University, Nanjing 210096, Jiangsu, China;* orcid.org/0000-0002-4648-2506

Complete contact information is available at: https://pubs.acs.org/10.1021/acs.jpcc.1c02029

Notes

The authors declare no competing financial interest.

■ ACKNOWLEDGMENTS

This work was supported by the Scientific Research Foundation of the Graduate School of Southeast University (YBPY2024), the Fundamental Research Funds for the Central Universities (2242017K41009, 2242018K41021), and the Science and Technology Support Program of Jiangsu Province (BE2018117).

■ REFERENCES

(1) Owen, J.; Brus, L. Chemical Synthesis and Luminescence Applications of Colloidal Semiconductor Quantum Dots. *J. Am. Chem. Soc.* **2017**, *139* (32), 10939–10943.

(2) Kagan, C. R.; Lifshitz, E.; Sargent, E. H.; Talapin, D. V. Building devices from colloidal quantum dots. *Science* **2016**, *353* (6302), aac5523.

(3) Dai, X. L.; Zhang, Z. X.; Jin, Y. Z.; Niu, Y.; Cao, H. J.; Liang, X. Y.; Chen, L. W.; Wang, J. P.; Peng, X. G. Solution-processed, high-performance light-emitting diodes based on quantum dots. *Nature* **2014**, *515* (7525), 96–99.

(4) Dang, C.; Lee, J.; Breen, C.; Steckel, J. S.; Coe-Sullivan, S.; Nurmikko, A. Red, green and blue lasing enabled by single-exciton gain in colloidal quantum dot films. *Nat. Nanotechnol.* **2012**, *7* (5), 335–339.

(5) Dang, C.; Lee, J.; Roh, K.; Kim, H.; Ahn, S.; Jeon, H.; Breen, C.; Steckel, J. S.; Coe-Sullivan, S.; Nurmikko, A. Highly efficient, spatially coherent distributed feedback lasers from dense colloidal quantum dot films (vol 103, 171104, 2013). *Appl. Phys. Lett.* **2013**, *103* (20), 209903.

(6) Klimov, V. I.; Mikhailovsky, A. A.; Xu, S.; Malko, A.; Hollingsworth, J. A.; Leatherdale, C. A.; Eisler, H. J.; Bawendi, M. G. Optical gain and stimulated emission in nanocrystal quantum dots. *Science* **2000**, *290* (5490), 314–317.

(7) Klimov, V. I.; Mikhailovsky, A. A.; McBranch, D. W.; Leatherdale, C. A.; Bawendi, M. G. Quantization of multiparticle

Auger rates in semiconductor quantum dots. *Science* **2000**, *287* (5455), 1011−1013.
(8) Climente, J. I.; Movilla, J. L.; Planelles, J. Auger Recombination Suppression in Nanocrystals with Asymmetric Electron-Hole Confinement. *Small* **2012**, *8* (5), 754−759.
(9) Garcia-Santamaria, F.; Brovelli, S.; Viswanatha, R.; Hollingsworth, J. A.; Htoon, H.; Crooker, S. A.; Klimov, V. I. Breakdown of Volume Scaling in Auger Recombination in CdSe/CdS Heteronanocrystals: The Role of the Core-Shell Interface. *Nano Lett.* **2011**, *11* (2), 687−693.
(10) Wang, L. W.; Califano, M.; Zunger, A.; Franceschetti, A. Pseudopotential theory of Auger processes in CdSe quantum dots. *Phys. Rev. Lett.* **2003**, *91* (5), 056404.
(11) Vaxenburg, R.; Rodina, A.; Shabaev, A.; Lifshitz, E.; Efros, A. L. Nonradiative Auger Recombination in Semiconductor Nanocrystals. *Nano Lett.* **2015**, *15* (3), 2092−2098.
(12) Fisher, B.; Caruge, J. M.; Zehnder, D.; Bawendi, M. Room-temperature ordered photon emission from multiexciton states in single CdSe core-shell nanocrystals. *Phys. Rev. Lett.* **2005**, *94* (8), 087403.
(13) Robel, I.; Gresback, R.; Kortshagen, U.; Schaller, R. D.; Klimov, V. I. Universal Size-Dependent Trend in Auger Recombination in Direct-Gap and Indirect-Gap Semiconductor Nanocrystals. *Phys. Rev. Lett.* **2009**, *102* (17), 177404.
(14) Walsh, B. R.; Saari, J. I.; Krause, M. M.; Nick, R.; Coe-Sullivan, S.; Kambhampati, P. Controlling the Surface of Semiconductor Nanocrystals for Efficient Light Emission from Single Excitons to Multiexcitons. *J. Phys. Chem. C* **2015**, *119* (28), 16383−16389.
(15) Guzelturk, B.; Kelestemur, Y.; Gungor, K.; Yeltik, A.; Akgul, M. Z.; Wang, Y.; Chen, R.; Dang, C.; Sun, H. D.; Demir, H. V. Stable and Low-Threshold Optical Gain in CdSe/CdS Quantum Dots: An All-Colloidal Frequency Up-Converted Laser. *Adv. Mater.* **2015**, *27* (17), 2741.
(16) Guo, W.; Tang, J.; Zhang, G.; Li, B.; Yang, C.; Chen, R.; Qin, C.; Hu, J.; Zhong, H.; Xiao, L.; Jia, S. Photoluminescence Blinking and Biexciton Auger Recombination in Single Colloidal Quantum Dots with Sharp and Smooth Core/Shell Interfaces. *J. Phys. Chem. Lett.* **2021**, *12* (1), 405−412.
(17) Javaux, C.; Mahler, B.; Dubertret, B.; Shabaev, A.; Rodina, A. V.; Efros, A. L.; Yakovlev, D. R.; Liu, F.; Bayer, M.; Camps, G.; Biadala, L.; Buil, S.; Quelin, X.; Hermier, J. P. Thermal activation of non-radiative Auger recombination in charged colloidal nanocrystals. *Nat. Nanotechnol.* **2013**, *8* (3), 206−212.
(18) Jain, A.; Voznyy, O.; Korkusinski, M.; Hawrylak, P.; Sargent, E. H. Ultrafast Carrier Trapping in Thick-Shell Colloidal Quantum Dots. *J. Phys. Chem. Lett.* **2017**, *8* (14), 3179−3184.
(19) Heyes, C. D.; Kobitski, A. Y.; Breus, V. V.; Nienhaus, G. U. Effect of the shell on the blinking statistics of core-shell quantum dots: A single-particle fluorescence study. *Phys. Rev. B: Condens. Matter Mater. Phys.* **2007**, *75* (12), 125431.
(20) Nguyen, T. L.; Michael, M.; Mulvaney, P. Synthesis of Highly Crystalline CdSe@ZnO Nanocrystals via Monolayer-by-Monolayer Epitaxial Shell Deposition. *Chem. Mater.* **2014**, *26* (14), 4274−4279.
(21) Walsh, B. R.; Saari, J. I.; Krause, M. M.; Mack, T. G.; Nick, R.; Coe-Sullivan, S.; Kambhampati, P. Interfacial Electronic Structure in Graded Shell Nanocrystals Dictates Their Performance for Optical Gain. *J. Phys. Chem. C* **2016**, *120* (34), 19409−19415.
(22) Minotto, A.; Todescato, F.; Fortunati, I.; Signorini, R.; Jasieniak, J. J.; Bozio, R. Role of Core-Shell Interfaces on Exciton Recombination in CdSe-CdxZn1-xS Quantum Dots. *J. Phys. Chem. C* **2014**, *118* (41), 24117−24126.
(23) Lim, J.; Park, Y. S.; Klimov, V. I. Optical gain in colloidal quantum dots achieved with direct-current electrical pumping. *Nat. Mater.* **2018**, *17* (1), 42.
(24) Wu, K. F.; Park, Y. S.; Lim, J.; Klimov, V. I. Towards zero-threshold optical gain using charged semiconductor quantum dots. *Nat. Nanotechnol.* **2017**, *12* (12), 1140.
(25) Fitzmorris, B. C.; Pu, Y. C.; Cooper, J. K.; Lin, Y. F.; Hsu, Y. J.; Li, Y.; Zhang, J. Z. Optical Properties and Exciton Dynamics of Alloyed Core/Shell/Shell Cd1-xZnxSe/ZnSe/ZnS Quantum Dots. *ACS Appl. Mater. Interfaces* **2013**, *5* (8), 2893−2900.
(26) Pu, Y. C.; Hsu, Y. J. Multicolored Cd1-xZnxSe quantum dots with type-I core/shell structure: single-step synthesis and their use as light emitting diodes. *Nanoscale* **2014**, *6* (7), 3881−3888.
(27) Beane, G. A.; Gong, K.; Kelley, D. F. Auger and Carrier Trapping Dynamics in Core/Shell Quantum Dots Having Sharp and Alloyed Interfaces. *ACS Nano* **2016**, *10* (3), 3755−3765.
(28) Garcia-Santamaria, F.; Chen, Y. F.; Vela, J.; Schaller, R. D.; Hollingsworth, J. A.; Klimov, V. I. Suppressed Auger Recombination in "Giant" Nanocrystals Boosts Optical Gain Performance. *Nano Lett.* **2009**, *9* (10), 3482−3488.
(29) Pu, Y. C.; Chen, W. T.; Fang, M. J.; Chen, Y. L.; Tsai, K. A.; Lin, W. H.; Hsu, Y. J. Au-Cd1-xZnxS core-alloyed shell nanocrystals: boosting the interfacial charge dynamics by adjusting the shell composition. *J. Mater. Chem. A* **2018**, *6* (36), 17503−17513.
(30) Zhao, J.; Chen, O.; Strasfeld, D. B.; Bawendi, M. G. Biexciton Quantum Yield Heterogeneities in Single CdSe (CdS) Core (Shell) Nanocrystals and Its Correlation to Exciton Blinking. *Nano Lett.* **2012**, *12* (9), 4477−4483.
(31) Omogo, B.; Gao, F.; Bajwa, P.; Kaneko, M.; Heyes, C. D. Reducing Blinking in Small Core-Multishell Quantum Dots by Carefully Balancing Confinement Potential and Induced Lattice Strain: The "Goldilocks" Effect. *ACS Nano* **2016**, *10* (4), 4072−4082.
(32) Li, B.; Zhang, G. F.; Zhang, Y.; Yang, C. G.; Guo, W. L.; Peng, Y. G.; Chen, R. Y.; Qin, C. B.; Gao, Y.; Hu, J. Y.; Wu, R. X.; Ma, J.; Zhong, H. Z.; Zheng, Y. J.; Xiao, L. T.; Jia, S. T. Biexciton Dynamics in Single Colloidal CdSe Quantum Dots. *J. Phys. Chem. Lett.* **2020**, *11* (24), 10425−10432.
(33) Bae, W. K.; Char, K.; Hur, H.; Lee, S. Single-step synthesis of quantum dots with chemical composition gradients. *Chem. Mater.* **2008**, *20* (2), 531−539.
(34) Yang, Y. X.; Zheng, Y.; Cao, W. R.; Titov, A.; Hyvonen, J.; Manders, J. R.; Xue, J. G.; Holloway, P. H.; Qian, L. High-efficiency light-emitting devices based on quantum dots with tailored nanostructures. *Nat. Photonics* **2015**, *9* (4), 259−266.
(35) Drijvers, E.; De Roo, J.; Geiregat, P.; Feher, K.; Hens, Z.; Aubert, T. Revisited Wurtzite CdSe Synthesis: A Gateway for the Versatile Flash Synthesis of Multishell Quantum Dots and Rods. *Chem. Mater.* **2016**, *28* (20), 7311−7323.
(36) Tang, J. L.; Huang, S.; Li, Z. H.; Shen, H. B.; Lv, Z.; Zhong, H. Z. Morphology Evolution of Gradient-Alloyed CdxZn1-xSeyS1-y@ZnS Core-Shell Quantum Dots during Transmission Electron Microscopy Determination: A Route to Illustrate Strain Effects. *J. Phys. Chem. C* **2018**, *122* (8), 4583−4588.
(37) Tang, J. L.; Li, F.; Yang, G. L.; Ge, Y.; Li, Z. H.; Xia, Z. G.; Shen, H. B.; Zhong, H. Z. Reducing the Chromaticity Shifts of Light-Emitting Diodes Using Gradient-Alloyed CdxZn1-xSeyS1-y@ZnS Core Shell Quantum Dots with Enhanced High-Temperature Photoluminescence. *Adv. Opt. Mater.* **2019**, *7* (10), 1801687.
(38) Acebron, M.; Galisteo-Lopez, J. F.; Lopez, C.; Herrera, F. C.; Mizrahi, M.; Requejo, F. G.; Palomares, F. J.; Juarez, B. H. Unexpected Optical Blue Shift in Large Colloidal Quantum Dots by Anionic Migration and Exchange. *J. Phys. Chem. Lett.* **2018**, *9* (11), 3124.
(39) Guzelturk, B.; Kelestemur, Y.; Akgul, M. Z.; Sharma, V. K.; Demir, H. V. Ultralow Threshold One-Photon- and Two-Photon-Pumped Optical Gain Media of Blue-Emitting Colloidal Quantum Dot Films. *J. Phys. Chem. Lett.* **2014**, *5* (13), 2214−2218.
(40) Cordones, A. A.; Leone, S. R. Mechanisms for charge trapping in single semiconductor nanocrystals probed by fluorescence blinking. *Chem. Soc. Rev.* **2013**, *42* (8), 3209−3221.
(41) Efros, A. L.; Nesbitt, D. J. Origin and control of blinking in quantum dots. *Nat. Nanotechnol.* **2016**, *11* (8), 661−671.
(42) Wu, K. F.; Lim, J.; Klimov, V. I. Superposition Principle in Auger Recombination of Charged and Neutral Multicarrier States in Semiconductor Quantum Dots. *ACS Nano* **2017**, *11* (8), 8437−8447.
(43) Zhang, L.; Li, H.; Liao, C.; Yang, H. Y.; Xu, R. L.; Jiang, X. S.; Xiao, M.; Lu, C. G.; Cui, Y. P.; Zhang, J. Y. New Insights into the

https://doi.org/10.1021/acs.jpcc.1c02029
J. Phys. Chem. C 2021, 125, 10759−10767

Multiexciton Dynamics in Phase-Pure Thick Shell CdSe/CdS Quantum Dots. *J. Phys. Chem. C* **2018**, *122* (43), 25059−25066.
(44) Bae, W. K.; Padilha, L. A.; Park, Y. S.; McDaniel, H.; Robel, I.; Pietryga, J. M.; Klimov, V. I. Controlled Alloying of the Core-Shell Interface in CdSe/CdS Quantum Dots for Suppression of Auger Recombination. *ACS Nano* **2013**, *7* (4), 3411−3419.
(45) Gong, K.; Kelley, D. F. Surface Charging and Trion Dynamics in CdSe-Based Core/Shell Quantum Dots. *J. Phys. Chem. C* **2015**, *119* (17), 9637−9645.
(46) Jha, P. P.; Guyot-Sionnest, P. Trion Decay in Colloidal Quantum Dots. *ACS Nano* **2009**, *3* (4), 1011−1015.
(47) Cragg, G. E.; Efros, A. L. Suppression of Auger Processes in Confined Structures. *Nano Lett.* **2010**, *10* (1), 313−317.
(48) Park, Y. S.; Bae, W. K.; Pietryga, J. M.; Klimov, V. I. Auger Recombination of Biexcitons and Negative and Positive Trions in Individual Quantum Dots. *ACS Nano* **2014**, *8* (7), 7288−7296.
(49) Huang, B.; Yang, H. Y.; Zhang, L.; Yuan, Y. F.; Cui, Y. P.; Zhang, J. Y. Effect of surface/interfacial defects on photo-stability of thick-shell CdZnSeS/ZnS quantum dots. *Nanoscale* **2018**, *10* (38), 18331−18340.
(50) Cihan, A. F.; Kelestemur, Y.; Guzelturk, B.; Yerli, O.; Kurum, U.; Yaglioglu, H. G.; Elmali, A.; Demir, H. V. Attractive versus Repulsive Excitonic Interactions of Colloidal Quantum Dots Control Blue- to Red-Shifting (and Non-shifting) Amplified Spontaneous Emission. *J. Phys. Chem. Lett.* **2013**, *4* (23), 4146−4152.
(51) Nanda, J.; Ivanov, S. A.; Achermann, M.; Bezel, I.; Piryatinski, A.; Klimov, V. I. Light amplification in the single-exciton regime using exciton-exciton repulsion in type-II nanocrystal quantum dots. *J. Phys. Chem. C* **2007**, *111* (42), 15382−15390.
(52) Wang, Y.; Li, X. M.; Nalla, V.; Zeng, H. B.; Sun, H. D. Solution-Processed Low Threshold Vertical Cavity Surface Emitting Lasers from All-Inorganic Perovskite Nanocrystals. *Adv. Funct. Mater.* **2017**, *27* (13), 1605088.
(53) Marra, D. C.; Aydil, E. S.; Joo, S. J.; Yoon, E.; Srdanov, V. I. Angle-dependent photoluminescence spectra of hydrogenated amorphous silicon thin films. *Appl. Phys. Lett.* **2000**, *77* (21), 3346−3348.

https://doi.org/10.1021/acs.jpcc.1c02029
J. Phys. Chem. C 2021, 125, 10759−10767